Available online at www.sciencedirect.com
SCIENCE DIRECT®
Applied Mathematical Modelling 29 (2005) 215–234
APPLIED MATHEMATICAL MODELLING
www.elsevier.com/locate/apm

Open-surface MHD flow over a curved wall in the 3-D thin-shear-layer approximation

S. Smolentsev *, M. Abdou

Department of Mechanical and Aerospace Engineering, Fusion Sciences and Technology Group, UCLA, 44-114 Engineering IV, 420 Westwood Pza, Los Angeles, CA 90095-1597, USA

Received 1 November 2002; received in revised form 1 May 2004; accepted 19 July 2004
Available online 13 October 2004

Abstract

3-D thin-shear-layer equations for flows of conducting fluids in a magnetic field have been derived in orthogonal body-oriented coordinates and then applied to the analysis of MHD open-surface flows over a curved wall. Unlike the classic boundary-layer-type equations, present ones permit information to be propagated upstream through the induced magnetic field. Another departure from the classic theory is that the normal momentum equation keeps the balance between the pressure gradient term, and those related to gravity, centrifugal forces, and Lorentz force. Thus, the normal pressure variations are allowed. The model describes basic 3-D effects due to the wall curvature and spatial variations of the applied magnetic field. As a particular case, equations for flows with rotational symmetry have been derived. Numerical calculations were performed for open-surface flows over a body of revolution under conditions relevant to a fusion reactor (Hartmann number is 8500). Some specific flow patterns, such as flow thickening and spiral-type flows, have been observed and discussed. A special attention has been paid to the analysis of the magnetic propulsion as a tool for the active flow control by applying an electric current. It has been shown that depending on the applied current, the axial pressure gradient can act as an adverse pressure gradient or propulsion force.

Keywords: Magnetohydrodynamics; Thin-shear-layer approximation; Free surface

* Corresponding author. Tel.: +1 310 794 5366; fax: +1 310 825 2599.
E-mail address: sergey@fusion.ucla.edu (S. Smolentsev).

0307-904X/$ - see front matter © 2004 Elsevier Inc. All rights reserved.
doi:10.1016/j.apm.2004.07.002

Nomenclature

Notation

Ha	Hartmann number
Re	Reynolds number
Re_{m}	magnetic Reynolds number
Fr	Froude number
$\mathbf{V}$	velocity vector (m/s)
$\mathbf{B}$	magnetic induction vector (T)
$\mathbf{j}$	current density vector (A/m^2)
$\mathbf{g}$	acceleration due to gravity(m/s^2)
G	pressure gradient (N/m^3)
H	metric coefficient (m)
J	current (A)
h	flow thickness (m)
K	curvature (m^{-1})
L, M, N	coefficients of the second fundamental form (m)
l	length scale along the flow (m)
P	pressure (N/m^2)
r	cylindrical radius (m)
t	time (s)
U, V, W	velocity components (m/s)
x, y	coordinates (m)

Greeks

θ	azimuthal angle
δ	length scale across the flow (m)
v	kinematic viscosity (m^2/s)
ρ	density (kg/m^3)
π	pi $= 3.141\ldots$
σ	electrical conductivity ($\Omega^{-1}\,m^{-1}$)
μ	magnetic permeability (H/m)
τ, ξ, η	dimensionless variables

1. Introduction

Open-surface flows of conducting liquids in a magnetic field are not unique in engineering applications. As examples we can refer to continuous casting of steel, where the liquid motion is controlled by a static magnetic field [12]. Another example is a liquid-wall flow in a fusion reactor. Recently, the liquid-wall concept has a significant place in the advanced power extraction (APEX) study [1]. In one of the APEX designs, liquid metal is injected poloidally at some location in the plasma chamber to form a thin liquid layer moving along the reactor walls. The layer

absorbs a high heat flux from the reactor plasma and through this protects the walls from overheating. In these flows, the characteristic flow length, l, far exceeds the typical length scale, δ, taken in the direction perpendicular to the main flow. For example, in the APEX liquid-wall flow, the characteristic flow thickness is of several centimeters, while the flow length, which is specified by the reactor chamber dimensions, is typically of several meters. Under these conditions, the transport phenomena in the main flow direction are mostly determined by convection. Thus, significant simplifications of the governing equations may be possible. The basis for the simplifications is the order of magnitude analysis that compares different terms in the dimensionless flow equations using δ/l as a scale. It has been known as a ''boundary-layer approximation''.

The boundary-layer equations were derived by Prandtl [21] for flows, in which the viscous layer near the solid surface is thin relative to the characteristic streamwise direction of the object immersed in the flow. More generally, the boundary-layer approximation is allowed for flows in which a primary flow direction can be identified. Other examples, rather than boundary layers, include jets, wakes, mixing layers, developing flows in pipes, and above mentioned open channel flows. Thus the terminology boundary-layer approximation has taken on a more general meaning, which refers to circumstances that permit the neglect of the transverse momentum equation and the streamwise second-derivative term in the remaining momentum equations. It is in a general practice at present, to refer to the flow equations written in the boundary-layer approximation as thin-shear-layer equations.

In classic hydrodynamics, both the 2-D and 3-D thin-shear-layer equations are used for flow calculations. The extension to 3-D flows introduces a number of special effects which are absent in the 2-D cases. The most distinctive effect is that a ''secondary flow'' is produced, in which the motion of the fluid departs from the main stream. This effect is usually related to the lateral body curvature. The other effect is the flow expansion or contraction due to the spatial deformations of the flow streamlines.

For non-MHD flows, 3-D thin-shear-layer equations have been derived by various methods by several authors. The most general equations for 3-D boundary layers were obtained in the classical study by Levi-Civita [13] who used non-orthogonal curvilinear coordinates. Other studies incorporated different coordinate systems, such as body-oriented orthogonal [8] and non-orthogonal [5] system, as well as streamline coordinate system [6]. Examples of application of the 3-D boundary-layer theory to different laminar non-MHD flows around curved surfaces are given in classic books [23,14,22,16]. More recently, [5] showed many results for turbulent 3-D boundary layers for wing-like and ship-like geometries. A particular case of 3-D thin-shear-layer equations is a flow with rotational symmetry [15]. This case is of considerable practical importance, and provides simplified examples of 3-D flows in which the flow quantities are independent of one of the space coordinate.

As for MHD open channel flows, the number of examples is sufficiently poorer. Strictly speaking, the MHD thin-shear-layer equations have not been presented yet in a systematical manner and their departure from analogous equations for non-MHD flows has not been emphasized either. Although the studies of open channel flows of conducting liquids in a magnetic field are great in number, many 3-D aspects of the flows have not been analyzed yet. The analyses of the open channel flows were conducted mostly for fully developed flows, in which the flow quantities do not experience downstream variations. The cases considered included the magnetic field perpendicular or inclined to the channel walls with a particular emphasis on the wall conductivity

effect [24,10,25,18]. The studies of developing flows are few in number and also do not include 3-D features, which are intrinsic in many MHD flows. Almost all of them were performed on the basis of the so-called ''averaged'' model (the most general form of the model was presented by Smolentsev [26,27]). The model is derived by integrating the 3-D governing equations along the direction of the applied magnetic field assuming the velocity and induced current distributions in the flow similar to those in the Hartmann layer. The calculations conducted were based on the boundary-layer approximation [2,7] and showed the impact of the Hartmann drag and flow opposing Lorentz force on the flow thickness and shape of the velocity profile. However, the model itself is quasi 2-D in character and restricted to relatively simple open channel flows, such as flows in an inclined chute in a one-component uniform magnetic field perpendicular to the chute walls. Hence, the averaged model cannot be considered as a good tool suited for studying more general cases complicated by such factors as curved geometry, multi-component magnetic field, and field spatial variations.

As an alternative to 2-D models, the full set of the 3-D Navier–Stokes–Maxwell equations can be used as the most general tool for the analysis of open channel MHD flows by solving the equations numerically. However, the numerical approach is severely restricted by the computer efficiency and capabilities of the present numerical methods. As a matter of fact, all numerical calculations of 3-D MHD flows based on the full set of governing equations reveal certain limitations on the flow parameters. In one of the first successful 3-D calculations performed for a closed channel flow in a magnetic field [29], the typical Hartmann number was only 50. More recent calculations [11] allowed higher Hartmann numbers ($Ha \sim 10^2$) but steel are not applicable to fusion problems where this parameter can be as high as 10^3–10^5.

In many cases, using the 3-D thin-shear-layer equations is a reasonable compromise between the 2-D approaches and those based on the full set of equations. If the criteria of the boundary-layer approximation are met, the approach can describe the most important 3-D flow features very well. Besides that, the computer codes that utilize the thin-shear-layer equations are relatively simple and can be applied to various flows under conditions relevant to real applications.

The primary object here is to find 3-D thin-shear-layer equations for MHD flows of incompressible liquid around a curved surface and then apply them to open-surface flows. The paper is organized in the following way. In Section 2, the governing Navier–Stokes–Maxwell equations are outlined as the starting point, then 3-D thin-shear-layer equations are derived in curvilinear body-oriented coordinates. A particular case of flows with rotational symmetry, such as flows over a body of revolution, is considered in Section 3. Section 4 introduces boundary conditions and specific details relevant to the open-surface flows. The numerical method used is explained in Section 5. Section 6 gives several numerical illustrations and their analysis for open-surface flows over a body of revolution in a multi-component magnetic field including the magnetic propulsion effect. Concluding remarks are formulated in Section 7.

2. General form of the 3-D MHD thin-shear-layer equations in body-oriented coordinates

When deriving the equations we restrict ourselves to laminar flows. Flow laminarization generally occurs in MHD flows where liquid metal is exposed to a strong magnetic field, such as a 10 T magnetic field in a fusion reactor. Based on the experimental data for channel flows, the

MHD flow becomes laminar if the parameter "the Hartmann number ($Ha = B_*\delta[\sigma/\nu\rho]^{1/2}$), over the Reynolds number ($Re = U_*\delta/\nu$)", exceeds its critical value [4]. Here U_* and B_* are characteristic velocity and applied magnetic field correspondingly, while σ, ν, and ρ are electrical conductivity, kinematic viscosity and fluid density. In what follows we will assume the condition, $Ha/Re > (Ha/Re)_{cr}$, is met and not introduce the turbulence effects in the model. Throughout the whole paper, we will also restrict our considerations to low-magnetic Reynolds number flows ($Re_m \ll 1$). The magnetic Reynolds number is defined here as $Re_m = \mu\sigma\delta U_*$, where μ is the magnetic permeability. Such flows widely occur in fusion and other applications using liquid metals, and molten salts. In the low-magnetic Reynolds number flows the magnetic field of the induced electric current is much smaller than the applied magnetic field.

If $\mathbf{V}$ is the velocity vector in the fluid, P is the pressure, $\mathbf{j}$ is the electric current density vector, $\mathbf{B}^0$ is the applied magnetic field, and ∇ denotes the gradient operator in 3-D, the governing flow equations of viscous incompressible, electrically conducting fluid with constant material properties in a magnetic field, can be written in the low-magnetic Reynolds number approximation in the following form:

$$\frac{\partial \mathbf{V}}{\partial t} + (\mathbf{V}\cdot\nabla)\mathbf{V} = -\frac{1}{\rho}\nabla P + \nu\nabla^2\mathbf{V} + \mathbf{g} + \frac{1}{\rho}\mathbf{j}\times\mathbf{B}^0, \tag{1}$$

$$\nabla\cdot\mathbf{V} = 0. \tag{2}$$

Here, $\mathbf{g}$ stands for the acceleration due to body forces different from the electromagnetic ones. Eq. (1) has been obtained by decomposing the magnetic field into the applied and induced parts:

$$\mathbf{B} = \mathbf{B}^0 + \mathbf{B}^i \tag{3}$$

and then neglecting the contribution of $\mathbf{B}^i$ to the Lorentz force. A group of electromagnetic equations includes Ampère's law, and the induction equation:

$$\mathbf{j} = \frac{1}{\mu}\nabla\times\mathbf{B}^i, \tag{4}$$

$$\frac{\partial \mathbf{B}^i}{\partial t} = \frac{1}{\mu\sigma}\nabla^2\mathbf{B}^i + (\mathbf{B}^0\cdot\nabla)\mathbf{V} - (\mathbf{V}\cdot\nabla)\mathbf{B}^0 - \frac{\partial \mathbf{B}^0}{\partial t}. \tag{5}$$

The induction equation is derived in a standard way [17] by applying the curl operator to Ohm's law and then substituting the electric field and the current by using Faraday's and Ampère's law. However unlike commonly accepted form of the induction equation in which the net magnetic field (3) is used as a variable, the present one is written through the induced magnetic field.

The following presentation will introduce the body-oriented orthogonal coordinates and deal with the equations in this particular coordinate system. The derivations are based on the use of notions and operators in vector analysis and differential geometry [31,32]; more recent [9]. The part of the discussion related to the flow equations is mostly adapted from [22].

The system of orthogonal curvilinear body-oriented coordinates is built as follows. The surface of the body is taken as the coordinate surface $x_2 = 0$, so that the coordinate lines x_2 are the curves

orthogonal to the surface. On the surface itself, the coordinate lines x_1 and x_3 are chosen in such a way to form an orthogonal net. Let H_1, H_2, H_3 and V_1, V_2, V_3 be the notations for the metric coefficients, and for the velocity vector components in directions of increasing x_1, x_2, x_3, respectively. Without loss of generality one can put $H_2 = 1$, so that the coordinate x_2 becomes simply the distance from the given point in the flow to the surface of the body.

By rejecting the terms, which are usually small in the boundary-layer approximation, the following projections of the momentum equation have been obtained:

$$\frac{\partial V_1}{\partial t} + \frac{V_1}{H_1}\frac{\partial V_1}{\partial x_1} + V_2\frac{\partial V_1}{\partial x_2} + \frac{V_3}{H_3}\frac{\partial V_1}{\partial x_3} + \frac{1}{H_1 H_3}\left(\frac{\partial H_1}{\partial x_3}V_1 V_3 - \frac{\partial H_3}{\partial x_1}V_3^2\right) = -\frac{1}{\rho}\frac{1}{H_1}\frac{\partial p}{\partial x_1} + g_1 + \nu\frac{\partial^2 V_1}{\partial x_2^2} + \frac{1}{\rho}(\mathbf{j}\times\mathbf{B}^0)_1, \tag{6}$$

$$\frac{L}{H_1^2}V_1^2 + \frac{2M}{H_1 H_3}V_1 V_3 + \frac{N}{H_3^2}V_3^2 - g_2 - \frac{1}{\rho}(\mathbf{j}\times\mathbf{B}^0)_2 = -\frac{1}{\rho}\frac{\partial p}{\partial x_2}, \tag{7}$$

$$\frac{\partial V_3}{\partial t} + \frac{V_1}{H_1}\frac{\partial V_3}{\partial x_1} + V_2\frac{\partial V_3}{\partial x_2} + \frac{V_3}{H_3}\frac{\partial V_3}{\partial x_3} + \frac{1}{H_1 H_3}\left(\frac{\partial H_3}{\partial x_1}V_1 V_3 - \frac{\partial H_1}{\partial x_3}V_3^2\right) = -\frac{1}{\rho}\frac{1}{H_3}\frac{\partial p}{\partial x_3} + g_3 + \nu\frac{\partial^2 V_3}{\partial x_2^2} + \frac{1}{\rho}(\mathbf{j}\times\mathbf{B}^0)_3. \tag{8}$$

The order of magnitude analysis used does not depart in essence from that for ordinary flows. As one can see, the second order derivatives parallel to the body surface have been neglected. All convection and diffusion terms in the normal momentum equation have also been neglected. The continuity equation reads

$$\frac{1}{H_1 H_3}\left[\frac{\partial(H_3 V_1)}{\partial x_1} + \frac{\partial(H_1 V_3)}{\partial x_3}\right] + \frac{\partial V_2}{\partial x_2} = 0. \tag{9}$$

Ampère's law reads

$$j_1 = \frac{1}{\mu}\frac{1}{H_3}\left[\frac{\partial(H_3 B_3^i)}{\partial x_2} - \frac{\partial B_2^i}{\partial x_3}\right], \quad j_2 = \frac{1}{\mu}\frac{1}{H_1 H_3}\left[\frac{\partial(H_1 B_1^i)}{\partial x_3} - \frac{\partial(H_3 B_3^i)}{\partial x_1}\right],$$
$$j_3 = \frac{1}{\mu}\frac{1}{H_1}\left[\frac{\partial B_2^i}{\partial x_1} - \frac{\partial(H_1 B_1^i)}{\partial x_2}\right]. \tag{10–12}$$

The projections of the induction equation were found as follows:

$$\frac{\partial B_1^i}{\partial t} = \mathbf{B}^0\cdot\nabla V_1 - \mathbf{V}\cdot\nabla B_1^0 + \frac{1}{H_1 H_3}\frac{\partial H_1}{\partial x_3}(B_1^0 V_3 - V_1 B_3^0) + \frac{1}{\mu\sigma}\nabla^2 B_1^i - \frac{\partial B_1^0}{\partial t}, \tag{13}$$

$$\frac{\partial B_2^i}{\partial t} = \mathbf{B}^0 \cdot \nabla V_2 - \mathbf{V} \cdot \nabla B_2^0 + \frac{1}{\mu\sigma}\nabla^2 B_2^i - \frac{\partial B_2^0}{\partial t}, \tag{14}$$

$$\frac{\partial B_3^i}{\partial t} = \mathbf{B}^0 \cdot \nabla V_3 - \mathbf{V} \cdot \nabla B_3^0 + \frac{1}{H_1 H_3}\frac{\partial H_3}{\partial x_1}(B_3^0 V_1 - V_3 B_1^0) + \frac{1}{\mu\sigma}\nabla^2 B_3^i - \frac{\partial B_3^0}{\partial t}. \tag{15}$$

In Eq. (7), L, M, and N are the coefficients of the second fundamental form of the surface. The Laplacian operator, and scalar products on the RHS of the equations, are expressed in terms of the coordinates x_1, x_2, x_3 as

$$\nabla^2 B_k^i = \frac{1}{H_1 H_3}\left[\frac{\partial}{\partial x_1}\left(\frac{H_3}{H_1}\frac{\partial B_k^i}{\partial x_1}\right) + \frac{\partial}{\partial x_2}\left(H_3 H_1 \frac{\partial B_k^i}{\partial x_2}\right) + \frac{\partial}{\partial x_3}\left(\frac{H_1}{H_3}\frac{\partial B_k^i}{\partial x_3}\right)\right],$$

$$\mathbf{B}^0 \cdot \nabla V_k = \frac{B_1^0}{H_1}\frac{\partial V_k}{\partial x_1} + B_2^0\frac{\partial V_k}{\partial x_2} + \frac{B_3^0}{H_3}\frac{\partial V_k}{\partial x_3}, \quad \text{and} \quad \mathbf{V} \cdot \nabla B_k^0 = \frac{V_1}{H_1}\frac{\partial B_k^0}{\partial x_1} + V_2\frac{\partial B_k^0}{\partial x_2} + \frac{V_3}{H_3}\frac{\partial B_k^0}{\partial x_3}.$$

Eq. (7) holds a number of terms, which are not necessarily negligible if $\delta/l \ll 1$. It expresses the balance between the pressure gradient effect, and those related to gravity, centrifugal forces, and the Lorentz force. Hence, the pressure is not constant in the x_2-direction. The other departure from the classic boundary-layer theory is that the system of equations is not fully parabolized. The presence of the induced magnetic field governed by Eqs. (13)–(15), that hold all the second derivatives, permits information to be propagated upstream. Retaining the second-derivative terms in the induction equation is a necessary step since the induced electric currents must be closed.

3. Case with rotational symmetry

Let us now consider flows with rotational symmetry, such as a flow over a body of revolution, assuming the applied magnetic field as well as the non-electromagnetic force, $\rho\mathbf{g}$, is also symmetrical. At present this case is of considerable practical importance for fusion applications, where the flow symmetry is allowed by the chamber topology. At the same time this case provides a simplified example of a 3-D flow in which the variables are independent of the azimuthal angle.

Here we will introduce the surface of revolution in a standard way as a surface generated by the rotation of a plane curve around an axis in its plane. The curvilinear body-oriented coordinates (Fig. 1) of any point P in the flow around the surface will be taken as (x, y, θ). Here θ is the angle between a fixed meridian plane and the meridian plain containing P; x is the distance OP' measured along a meridian curve from the nose O or another characteristic point at the surface to the projection $P'$of P onto the surface; y is the distance $P'P$ measured along the normal from the surface. These coordinates form a set of orthogonal coordinates fitted to the surface of the body. Let U, V, W be the components of velocity of the fluid at P, in directions of increasing x, y, and θ, respectively. If r is the distance of P' from the axis of revolution, so that r is a function of x alone,

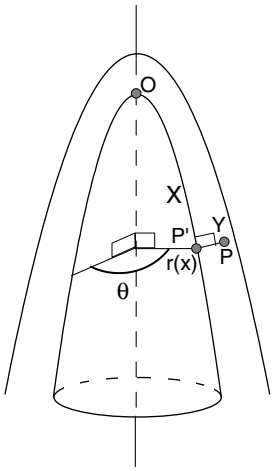

Fig. 1. The coordinate system for open-channel flow over a body of revolution.

then in the notation used, $H_1 = 1$, and $H_3 = r$. As for the applied magnetic field, it can be considered to be independent on y, because its variations across the flow thickness are insignificant by virtue of $\delta/l \ll 1$.

We can immediately take the advantage of axial symmetry by expressing the azimuthal current from Ohm's law ($\mathbf{j} = \sigma[-\nabla\varphi + \mathbf{V} \times \mathbf{B}^0]$, where φ is the electric potential), such that

$$j_\theta = \sigma(\mathbf{V} \times \mathbf{B}^0)_\theta = \sigma(UB_y^0 - VB_x^0). \tag{16}$$

The two other current components are calculated using Ampère's law

$$j_x = \frac{1}{\mu}\frac{\partial B_\theta^i}{\partial y}, \quad j_y = -\frac{1}{\mu}\frac{1}{r}\frac{\partial (rB_\theta^i)}{\partial x}. \tag{17,18}$$

Thus, to calculate the electric current, only the azimuthal component of the magnetic field is required, which can be calculated from the following induction equation

$$\frac{\partial B_\theta^i}{\partial t} = B_x^0\frac{\partial W}{\partial x} + B_y^0\frac{\partial W}{\partial y} - \left(\frac{\mathrm{d}B_\theta^0}{\mathrm{d}x} - \frac{B_\theta^0}{r}\frac{\mathrm{d}r}{\mathrm{d}x}\right)U - \frac{WB_x^0}{r}\frac{\mathrm{d}r}{\mathrm{d}x} + \frac{1}{\mu_0\sigma}\left[\frac{1}{r}\frac{\partial}{\partial x}\left(r\frac{\partial B_\theta^i}{\partial x}\right) + \frac{\partial^2 B_\theta^i}{\partial y^2}\right] - \frac{\partial B_\theta^0}{\partial t}. \tag{19}$$

The flow equations are directly obtained from Eqs. (6)–(9) as follows

$$\frac{\partial U}{\partial t} + U\frac{\partial U}{\partial x} + V\frac{\partial U}{\partial y} - \frac{W^2}{r}\frac{\mathrm{d}r}{\mathrm{d}x} = -\frac{1}{\rho}\frac{\partial p}{\partial x} + g_x + \nu\frac{\partial^2 U}{\partial y^2} + \frac{1}{\rho}(j_y B_\theta^0 - j_\theta B_y^0), \tag{20}$$

$$\rho(K_a U^2 + K_b W^2 + g_y) + (j_\theta B_x^0 - j_x B_\theta^0) = \frac{\partial p}{\partial y}, \tag{21}$$

$$\frac{\partial W}{\partial t} + U\frac{\partial W}{\partial x} + V\frac{\partial W}{\partial y} + \frac{UW}{r}\frac{\mathrm{d}r}{\mathrm{d}x} = g_\theta + \nu\frac{\partial^2 W}{\partial y^2} + \frac{1}{\rho}(j_x B_y^0 - j_y B_x^0), \tag{22}$$

$$\frac{1}{r}\frac{\partial (rU)}{\partial x} + \frac{\partial V}{\partial y} = 0. \tag{23}$$

Here $1/K_a$ and $1/K_b$ are the two principal radii of curvature. K_a is the curvature of the generating curve, being positive when the wall is convex outwards and negative when it is concave outwards. K_b is the reciprocal of the length of the normal intercepted between the curve and the axis of rotation.

4. Open-surface flow over a body of revolution

The following discussion will deal with open-surface flows over a body of revolution. To eliminate the pressure, we integrate Eq. (21) from y to the local flow thickness h. Then the equation obtained is differentiated with respect to x to give an equation for the axial pressure gradient as follows

$$-\frac{1}{\rho}\frac{\partial p(x,y)}{\partial x} = -\frac{1}{\rho}\frac{\mathrm{d}p|_{y=h}}{\mathrm{d}x} - \frac{1}{\rho}B_\theta^0 j_y + G_1 + G_2 - \frac{1}{\rho}B_\theta^0\left(j_x|_{y=h}\frac{\partial h}{\partial x} - j_y|_{y=h}\right), \tag{24}$$

$$G_1 = \frac{\partial}{\partial x}\int_y^h \left(K_a U^2 + K_b W^2 + g_y + \frac{\sigma}{\rho}(UB_y^0 - VB_x^0)B_x^0\right)\mathrm{d}y,$$
$$G_2 = \frac{1}{\rho\mu_0}\left(\frac{\mathrm{d}B_\theta^0}{\mathrm{d}x} - \frac{B_\theta^0}{r}\frac{\mathrm{d}r}{\mathrm{d}x}\right)(B_\theta^i - B_\theta^i|_{y=h}). \tag{25}$$

When deriving (24) it was assumed that the free surface deformations over the characteristic length δ are moderate so that the pressure at the free surface does not differ from the atmospheric pressure. The term G_1 is a positive part of the pressure gradient, while G_2 is either positive or negative. If the pressure at the free surface does not vary with x, the first term on the RHS of Eq. (24) is equal to zero. The last term is also equal to zero since the electric current at the free surface is tangential to the surface. After substitution the pressure gradient from Eq. (24) in Eq. (20), term $-\rho^{-1}B_\theta^0 j_y$ is canceled, and Eq. (20) takes the following form

$$\frac{\partial U}{\partial t} + U\frac{\partial U}{\partial x} + V\frac{\partial U}{\partial y} - \frac{W^2}{r}\frac{\mathrm{d}r}{\mathrm{d}x} = G_1 + G_2 + g_x + \nu\frac{\partial^2 U}{\partial y^2} - \frac{\sigma}{\rho}(UB_y^0 - VB_x^0)B_y^0. \tag{26}$$

To close the problem one more equation for tracking the free surface should be added, such as the kinematic free surface condition:

$$\frac{\partial h}{\partial t} + U_h \frac{\partial h}{\partial x} = V_h. \tag{27}$$

Here U_h and V_h are the velocity components taken at the free surface. The final set of equations includes Eqs. (17)–(19) that represent the electromagnetic part, and the flow equations (22) and (23), (25)–(27).

As for the boundary conditions, no-slip and no-tangential stress conditions are used at the rigid boundary and at the free surface, respectively, with an appropriate velocity profile in the initial cross-section. The formulation of boundary conditions on B^i_θ is based on the continuity of the electric current. We do not consider electrically conducting walls, so that all induced currents take their path within the flow domain. We also assume that some voltage can be applied between the inlet and outlet sections resulting in the axial electric current, J, such that

$$J = 2\pi r \int_0^h j_x(x,y)\,\mathrm{d}y = \frac{2\pi r}{\mu}\left(B^i_\theta|_{y=h} - B^i_\theta|_{y=0}\right). \tag{28}$$

Using Eq. (28), the boundary conditions on B^i_θ, that assure solenoidal electric current in the flow domain, are formulated as follows:

$$\begin{aligned}
&x = 0 \text{ (inlet)}, \quad 0 \leqslant y \leqslant h(0): \quad B^i_\theta = \frac{\mu_0 J}{2\pi r(0)h(0)} \int_0^y f_0(y)\,\mathrm{d}y,\\
&x = l \text{ (outlet)}, \quad 0 \leqslant y \leqslant h(l): \quad B^i_\theta = \frac{\mu_0 J}{2\pi r(l)h(l)} \int_0^y f_l(y)\,\mathrm{d}y,\\
&y = 0 \text{ (rigid wall)}, \quad 0 \leqslant x \leqslant l: \quad B^i_\theta = 0,\\
&y = h \text{ (free surface)}, \quad 0 \leqslant x \leqslant l: \quad B^i_\theta = \frac{\mu_0 J}{2\pi r(x)}.
\end{aligned} \tag{29}$$

Here, $f_0(y)$ and $f_l(y)$ are two form-functions, such that $\frac{1}{h}\int_0^h f\,\mathrm{d}y = 1$, which stand for the distribution of the applied current across the liquid layer at the flow inlet and outlet, respectively. In what follows we will assume that these distributions are uniform: $f_0(y) = f_l(y) = 1$.

The peculiar feature of flows considered is that they experience MHD forces resulting mostly from the axial induced currents. These currents appear as a result of the MHD interaction due to spatial changes in B^0_θ or can be caused by geometrical changes, such as variations in the flow direction. As it was recognized earlier [17] these two cases are similar by nature. However, this conclusion was drawn based on the observation of results for various MHD flows. It is noticeable, that the present equations show the similarity directly, as the same expression, $\mathrm{d}B^0_\theta/\mathrm{d}x - B^0_\theta r^{-1}\mathrm{d}r/\mathrm{d}x$, enters both the momentum equation and induction equation. The first term in this expression, as it is easy to see, stands for the space variation of a magnetic field, while the second term appears due to geometrical changes. In the case of a "$1/r$" magnetic field ($B^0_\theta = B_* r_*/r$), which is a typical magnetic field in a fusion reactor,

$$\frac{\mathrm{d}B^0_\theta}{\mathrm{d}x} = B^0_\theta \frac{1}{r}\frac{\mathrm{d}r}{\mathrm{d}x} - \frac{B_* r_*}{r^2}\frac{\mathrm{d}r}{\mathrm{d}x},$$

so that the field variation effect and that due to the geometrical changes become equally important.

The set of equations presented in this section is full because it contains five equations that determine five unknowns, U, V, W, B^i_θ, and h. Although the equations are relatively simple, they can hardly be solved analytically because of the non-linear terms, and temporal as well as spatial variations of the boundaries of the flow domain. However numerical treatment should present no problems and is much simpler than solving the full set of the 3-D Navier–Stokes–Maxwell equations. The numerical method and some calculations are shown in the next sections.

5. Numerical method

It is useful to choose dimensionless variables by taking proper scales. We use h_0 (the inlet flow thickness) as a length scale, U_0 (the average inlet velocity) as a velocity scale, B_0 (the magnitude of the azimuthal magnetic field in the flow inlet) as an applied magnetic field scale, and $Re_m B_0$ as a scale for the induced magnetic field. New independent variables are introduced, such as $\tau = tU_0/h_0$, $\xi = x/h_0$, and $\eta = y/h(x)$. By using these variables, the curvilinear flow domain in the physical plane (x,y) is reduced to the rectangular domain in the computational plane (ξ,η). The dimensional quantities are scaled by the characteristic values in the following form: $\widetilde{\mathbf{V}} = \mathbf{V}/U_0$, $\widetilde{\mathbf{B}}^0 = \mathbf{B}^0/B_0$, $\widetilde{\mathbf{B}}^i = \mathbf{B}^i/(Re_m B_0)$ $\tilde{h} = h/h_0$, $\tilde{r} = r/h_0$, and $\widetilde{K} = K/(h_0^{-1})$. The relevant dimensionless groups are the Reynolds number ($Re = U_0 h_0/\nu$), Froude number ($Fr = U_0^2/[gh_0]$), Hartmann number ($Ha = B_0 h_0[\sigma/(\nu\rho)]^{0.5}$), and the magnetic Reynolds numberz ($Re_m = U_0 h_0 \mu_0 \sigma$). Then, the governing equations for the open-surface flow over a body of revolution take the following form

$$\left(\frac{\partial \widetilde{U}}{\partial \tau} - \eta\frac{\dot{\tilde{h}}}{\tilde{h}}\frac{\partial \widetilde{U}}{\partial \eta}\right) + \widetilde{U}\left(\frac{\partial \widetilde{U}}{\partial \xi} - \eta\frac{\tilde{h}'}{\tilde{h}}\frac{\partial \widetilde{U}}{\partial \eta}\right) + \frac{\widetilde{V}}{\tilde{h}}\frac{\partial \widetilde{U}}{\partial \eta} - \widetilde{W}^2\frac{\tilde{r}'}{\tilde{r}}$$
$$= \widetilde{G}_1 + \widetilde{G}_2 + \frac{1}{Fr}\frac{g_x}{g} + \frac{1}{Re}\frac{1}{\tilde{h}^2}\frac{\partial^2 \widetilde{U}}{\partial \eta^2} - \frac{Ha^2}{Re}(\widetilde{U}\widetilde{B}^0_y - \widetilde{V}\widetilde{B}^0_x)\widetilde{B}^0_y, \tag{30}$$

$$\widetilde{G}_1 = \frac{\partial}{\partial \xi}\tilde{h}\int_\eta^1 \left[\widetilde{K}_a\widetilde{U}^2 + \widetilde{K}_b\widetilde{W}^2 + \frac{1}{Fr}\frac{g_y}{g} + \frac{Ha^2}{Re}(\widetilde{U}\widetilde{B}^0_y - \widetilde{V}\widetilde{B}^0_x)\widetilde{B}^0_x\right] d\eta,$$

$$\widetilde{G}_2 = \frac{Ha^2}{Re}\left(\frac{d\widetilde{B}^0_\theta}{d\xi} - \frac{\tilde{r}'}{\tilde{r}}\widetilde{B}^0_\theta\right)(\widetilde{B}^i_\theta - \widetilde{B}^i_\theta|_{\eta=1}),$$

$$\left(\frac{\partial \widetilde{W}}{\partial \tau} - \eta\frac{\dot{\tilde{h}}}{\tilde{h}}\frac{\partial \widetilde{W}}{\partial \eta}\right) + \widetilde{U}\left(\frac{\partial \widetilde{W}}{\partial \xi} - \eta\frac{\tilde{h}'}{\tilde{h}}\frac{\partial \widetilde{W}}{\partial \eta}\right) + \frac{\widetilde{V}}{\tilde{h}}\frac{\partial \widetilde{W}}{\partial \eta} + \widetilde{U}\widetilde{W}\frac{\tilde{r}'}{\tilde{r}}$$
$$= \frac{1}{Fr}\frac{g_\theta}{g} + \frac{1}{Re}\frac{1}{\tilde{h}^2}\frac{\partial^2 \widetilde{W}}{\partial \eta^2} + \frac{Ha^2}{Re}\left\{\frac{1}{\tilde{h}}\frac{\partial \widetilde{B}^i_\theta}{\partial \eta}B^0_y + \frac{1}{\tilde{r}}\left[\frac{\partial(\tilde{r}\widetilde{B}^i_\theta)}{\partial \xi} - \eta\frac{\tilde{h}'}{\tilde{h}}\frac{\partial(r\widetilde{B}^i_\theta)}{\partial \eta}\right]\widetilde{B}^0_x\right\}, \tag{31}$$

$$\frac{1}{\tilde{r}}\left[\frac{\partial(\tilde{r}\widetilde{U})}{\partial\xi}-\eta\frac{\tilde{h}'}{\tilde{h}}\frac{\partial(\tilde{r}\widetilde{U})}{\partial\eta}\right]+\frac{1}{\tilde{h}}\frac{\partial\widetilde{V}}{\partial\eta}=0, \tag{32}$$

$$\begin{aligned}Re_{\mathrm{m}}\left(\frac{\partial\widetilde{B}^{i}_{\theta}}{\partial\tau}-\eta\frac{\dot{\tilde{h}}}{\tilde{h}}\frac{\partial\widetilde{B}^{i}_{\theta}}{\partial\eta}\right)&=\widetilde{B}^{0}_{x}\left(\frac{\partial\widetilde{W}}{\partial\xi}-\eta\frac{\tilde{h}'}{\tilde{h}}\frac{\partial\widetilde{W}}{\partial\eta}\right)+\frac{\widetilde{B}^{0}_{y}}{\tilde{h}}\frac{\partial\widetilde{W}}{\partial\eta}-\left(\frac{\mathrm{d}\widetilde{B}^{0}_{\theta}}{\mathrm{d}\xi}-\frac{\tilde{r}'}{\tilde{r}}\widetilde{B}^{0}_{\theta}\right)\widetilde{U}-\widetilde{W}\widetilde{B}^{0}_{x}\frac{\tilde{r}'}{\tilde{r}}\\&+\frac{1}{\tilde{r}}\frac{\partial}{\partial\xi}\left(\tilde{r}\frac{\partial\widetilde{B}^{i}_{\theta}}{\partial\xi}\right)+\eta\left(\frac{2\tilde{h}'^{2}-\tilde{h}\tilde{h}''}{\tilde{h}^{2}}-\frac{\tilde{h}'}{\tilde{h}}\frac{\tilde{r}'}{\tilde{r}}\right)\frac{\partial\widetilde{B}^{i}_{\theta}}{\partial\eta}-2\eta\frac{\tilde{h}'}{\tilde{h}}\frac{\partial^{2}\widetilde{B}^{i}_{\theta}}{\partial\xi\partial\eta}\\&+\left[\left(\eta\frac{\tilde{h}'}{\tilde{h}}\right)^{2}+\frac{1}{\tilde{h}^{2}}\right]\frac{\partial^{2}\widetilde{B}^{i}_{\theta}}{\partial\eta^{2}}-\frac{\partial\widetilde{B}^{0}_{\theta}}{\partial\tau},\end{aligned} \tag{33}$$

$$\dot{\tilde{h}}+\widetilde{U}_{h}\tilde{h}'=\widetilde{V}_{h}. \tag{34}$$

Here $\dot{\tilde{h}}$ and $\tilde{h}'$ are used as a notation for partial derivatives $\partial\tilde{h}/\partial\tau$ and $\partial\tilde{h}/\partial\xi$, respectively. The dimensionless form of the boundary conditions is as follows

$$\begin{aligned}&\xi=0,\quad 0\leqslant\eta\leqslant 1:\quad \widetilde{B}^{i}_{\theta}=\widetilde{J}\eta/\tilde{r}(0),\\&\xi=\tilde{l},\quad 0\leqslant\eta\leqslant 1:\quad \widetilde{B}^{i}_{\theta}=\widetilde{J}\eta/\tilde{r}(\tilde{l}),\\&\eta=0,\quad 0\leqslant\xi\leqslant l/h_{0}:\quad \widetilde{B}^{i}_{\theta}=0,\\&\eta=1,\quad 0\leqslant\xi\leqslant l/h_{0}:\quad \widetilde{B}^{i}_{\theta}=\widetilde{J}/\tilde{r}(\xi),\end{aligned} \tag{35}$$

where $\tilde{l}=l/h_{0}$, and $\widetilde{J}=\frac{\mu_{0}}{2\pi h_{0}B_{0}}J$ is the re-scaled applied current.

In what follows, we will assume that the applied magnetic field does not vary in time, thus a steady flow regime can be achieved. The steady solution is obtained by advancing in time. A slug-type flow, constant flow thickness, and zero induced magnetic field are used as an initial guess. All equations are approximated implicitly with finite-difference formulas using the finite-volume approach on a non-uniform rectangular mesh that clusters grid points near the rigid boundary and free surface, where the flow and magnetic field gradients are expected to be higher. The grid clustering were performed using the stretching transformation for the boundary-layer-type of problems. If the mesh is uniform, the finite-difference scheme provides the second-order approximation with respect to both ξ and η. The two momentum equations are solved by the Blottner-type technique [3], which is well suited for marching problems. The induction equation is solved with the help of the ADI method [20]. The height function approach [19] is used for tracking the free surface. A similar numerical method for solving marching problems was used by authors in calculations of MHD turbulent open channel flows [28]. This method demonstrated high accuracy as well as good convergence in a wide range of

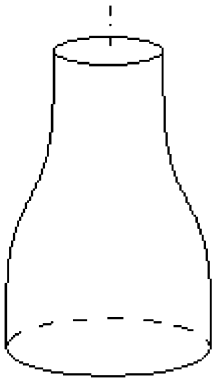

Fig. 2. The "bottle-neck" surface of revolution.

flow parameters. Other free surface tracking techniques, such as volume of fluid or level-set method, can also be applied but their use for the boundary-layer-type of problems does not give any advantages and requires more computational time in comparison with the simpler height function method.

All calculations were conducted for a flow around a "bottle-neck" surface of revolution (Fig. 2). Typical flow parameters are shown in Fig. 4. The surface of revolution was generated by a curve

$$\tilde{r}(\xi) = a + \tanh\{b \times (\xi - c)\}, \tag{36}$$

where a, b, and c are the dimensionless shape factors. Several grids, such as 75×51 (A), 101×75 (B), and 251×101 (C) were tested. The results obtained with grids B and C are almost identical, so that grid B was used in almost all calculations. The time increment does not affect the steady-state solution. A relatively big $\Delta\tau = 5$ was chosen to reduce the computational time. The convergence criterion was constructed as $|(\tilde{h}^n - \tilde{h}^{n-1})/\tilde{h}^n| < \varepsilon$, where n is the iteration number and $\varepsilon = 10^{-7}$. To satisfy this criterion, from 600 to 1000 iterations were required. All computations were performed with a PC (Intel Pentium 4, 2.26 GHz) using double precision. The model developed allows for very fast calculations, which do not take more than a few minutes. The maximum Hartmann number resolved in the present calculations was 8500. It should be noted that numerical calculations of simpler MHD flows based on the full 3-D models usually take tens of hours to perform calculations at much more moderate Hartmann numbers.

6. Results

The liquid driven by a gravity force flows down over the surface forming a thin liquid layer. As a prototype of such a flow we can refer to a liquid-metal flow around the central column of a low-aspect ratio fusion reactor [33]. A two-component magnetic field, $(0, B_y^0, B_\theta^0)$, is applied. The axial component, which is parallel to the main flow direction, has not been included since it is expected

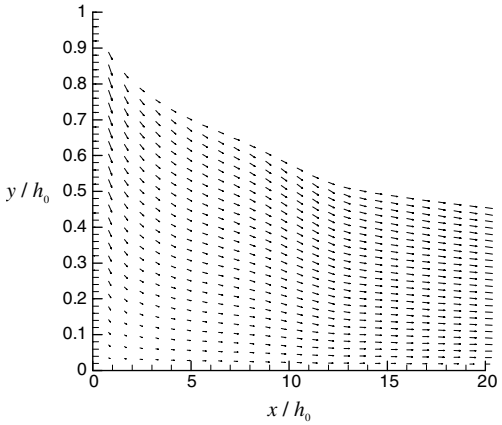

Fig. 3. Flow without a magnetic field. Velocity vector plot in the x–y plane. Changes are due to the gravity force and flow expansion. $Re = 23500$, $Fr = 5$.

to have a weaker impact on the flow than the other two. To emphasize relevance to reactor conditions, the azimuthal component of the magnetic field has been taken as "$1/r$", such that

$$\widetilde{B}_{\theta}^{0} = \frac{a + \tanh\{-b \times c\}}{\tilde{r}(\xi)}. \tag{37}$$

The wall-normal magnetic field has been taken constant, so that the applied magnetic field satisfies the magnetostatic equations, i.e. $\nabla \times \mathbf{B}^0 = 0$, and $\nabla \cdot \mathbf{B}^0 = 0$. Hence, such a field can really exist and be realized in an experiment or even under real reactor conditions. The case without a magnetic field is illustrated in Fig. 3. The flow thickness is monotonically reduced by the gravity and due to the flow expansion. The only 3-D effect is one of flow divergence or convergence. That is

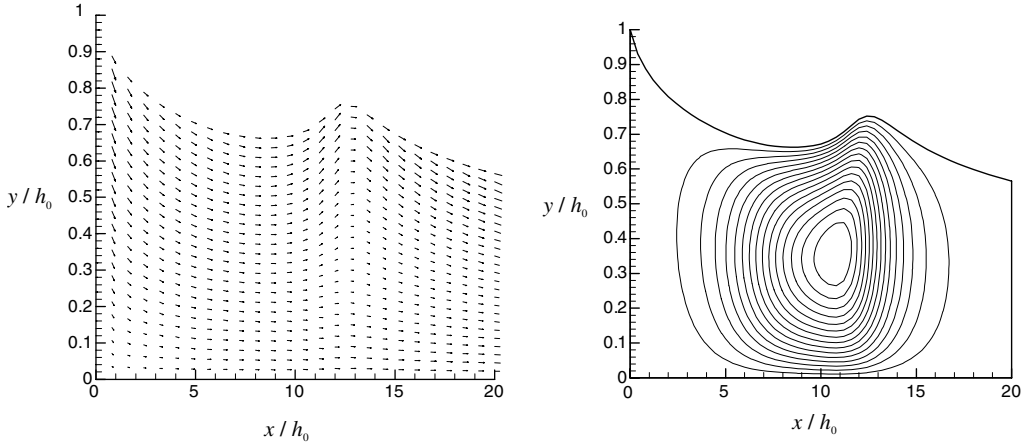

Fig. 4. Flow with an azimuthal magnetic field. Left: velocity vector plot. Right: induced magnetic field counter lines. $Re = 23500$, $Fr = 5$, $Ha = 8500$.

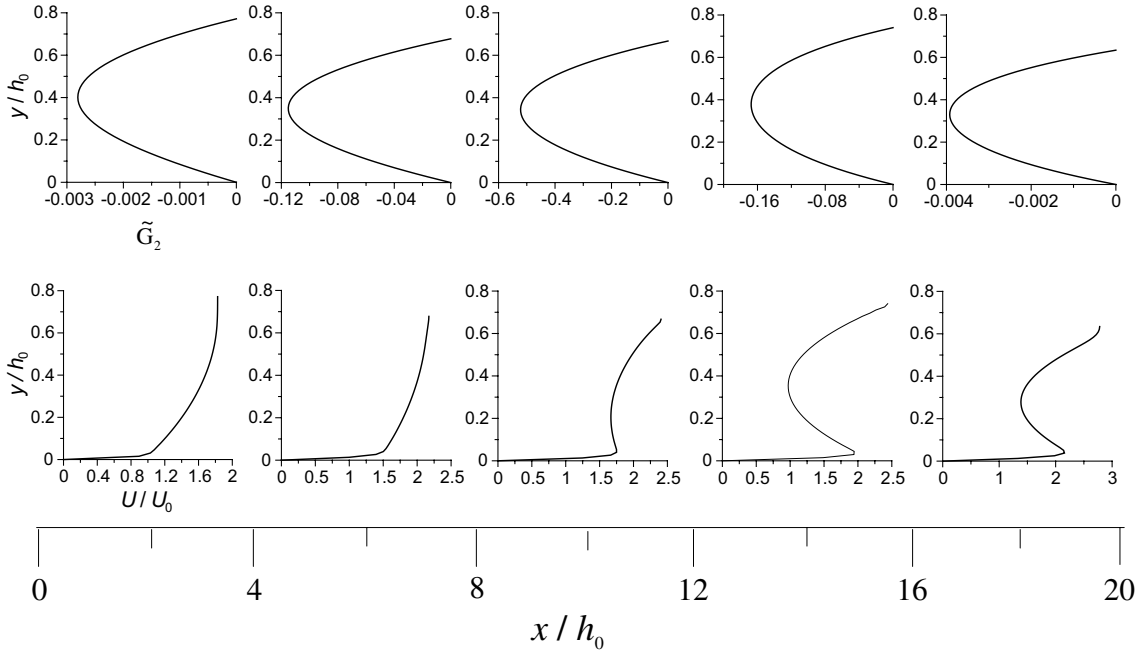

Fig. 5. Downstream variations of the velocity profile (lower) and adverse pressure gradient (upper). See parameters in Fig. 4.

the surface geometry causes a stretching (or contraction) of the streamlines of the main flow that results in a thinning (or thickening) of the layer.

As a first illustration of MHD effects, we will consider a flow with an azimuthal magnetic field only. Electric currents are induced in the x–y plane and electromagnetic forces are located in the same plane. In the area where the body expands and the magnetic field also experiences major changes, these forces drive the liquid out of the flow bulk towards the free surface. This typically results in a "surface bump" (Fig. 4). The induced electric current takes its path within the flow domain and is stronger near the back-wall and free surface. The velocity profiles within the bump area and downstream of the bump take the characteristic M-shape similar to those in electrically conducting rectangular ducts in a constant transverse magnetic field (Fig. 5). These effects are related to the negative part (G_2) of the pressure gradient term, which acts as an adverse pressure gradient. Its distribution across the layer (Fig. 6) is near parabolic with the maximum at the point about halfway between the rigid wall and free surface. The results at weaker magnetic fields ($Ha < 8500$) showed smaller bumps and less pronounced non-uniformity of the velocity profile. However, all computer runs attempted with $Ha > 9000$ resulted in a "run-time error" that most likely points to the model inapplicability if the surface disturbances are significant. All analyses beyond this limit will require higher order approximations in the flow equations rather than marching type flow equations adopted in the present approach. As an intermediate model between the present one and the full 3-D set of equations, which is most likely is a good choice for flows at higher Ha, we could suggest the "parabolozed" Navier–Stokes equations [30].

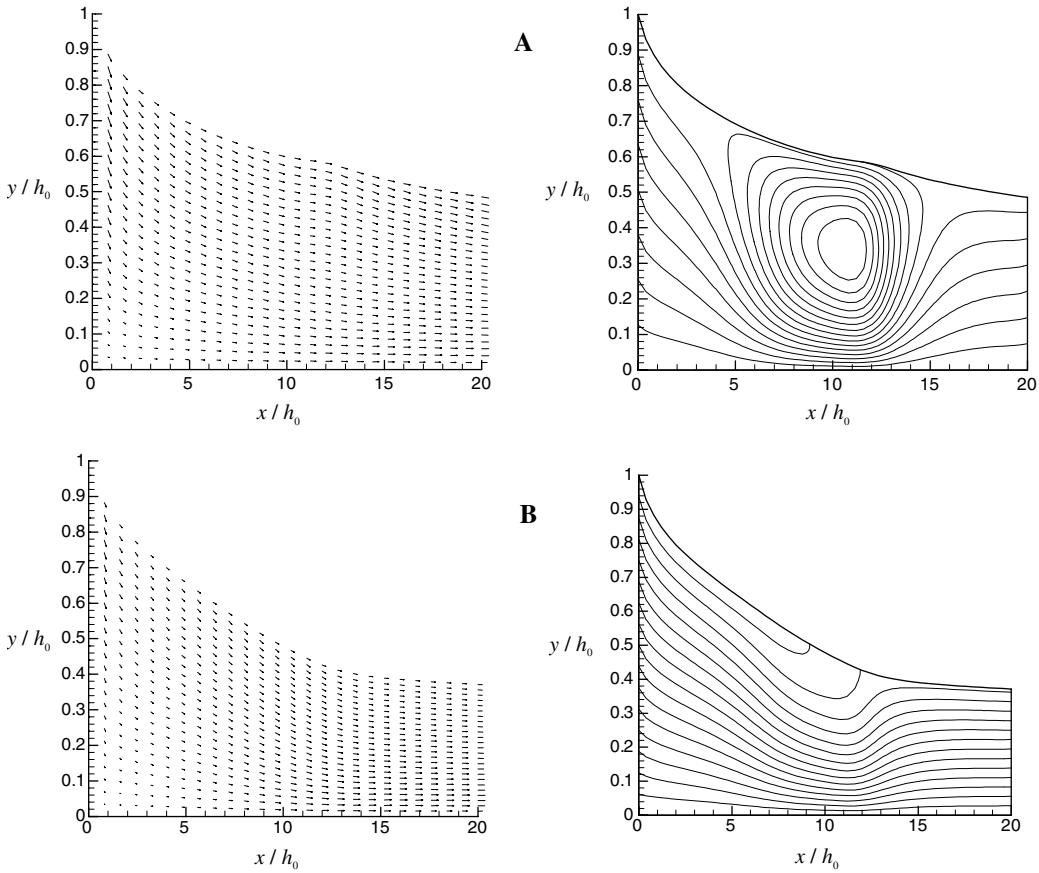

Fig. 6. Effect of the applied electric current on the flow. See parameters in Fig. 3. (A) $\widetilde{J} = 2.0 \times 10^{-3}$; (B) $\widetilde{J} = 1.0 \times 10^{-2}$.

The next example illustrates the idea of so-called ''magnetic propulsion''. A concept of magnetic propulsion for liquid-metal streams in a tokomak reactor was proposed by Zakharov et al. [34]. In accordance with the concept, an axial electric current is injected into the liquid layer. The current interacts with a non-uniform reactor magnetic field giving a rise to a propulsion force. The propulsion effect can directly be seen from Eq. (30). In the absence of an external current ($\widetilde{B}^{i}_{\theta} = 0$), the term $\widetilde{G}_2$ is negative and acts as an adverse pressure gradient. However, with an applied current, $\widetilde{G}_2$ changes its sign and starts acting as a propulsion force. The present calculations (Fig. 7) illustrate details of the magnetic propulsion effect. They are in a good agreement with the qualitative analysis presented earlier by Zakharov et al. However, present considerations also show that the propulsion force can originate not only from the non-uniformity of the magnetic field but also from the wall curvature. It can directly be seen from the $\widetilde{G}_2$ term on the RHS of Eq. (30). It is more appropriate to say that the propulsion mechanism owes its existence to changes of both the magnetic field and flow geometry. The induced and applied electric currents are responsible for two opposite mechanisms that determine the shape of the free surface. The

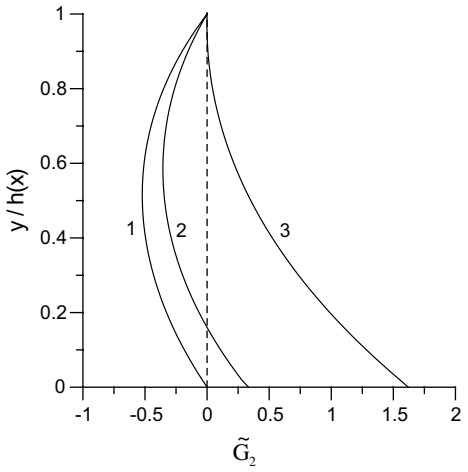

Fig. 7. Transition from adverse pressure gradient flow (1) to flow with acceleration (3) due to magnetic propulsion. See parameters in Fig. 4. (1) $\widetilde{J} = 0$; (2) $\widetilde{J} = 2.0 \times 10^{-3}$; (3) $\widetilde{J} = 1.0 \times 10^{-2}$.

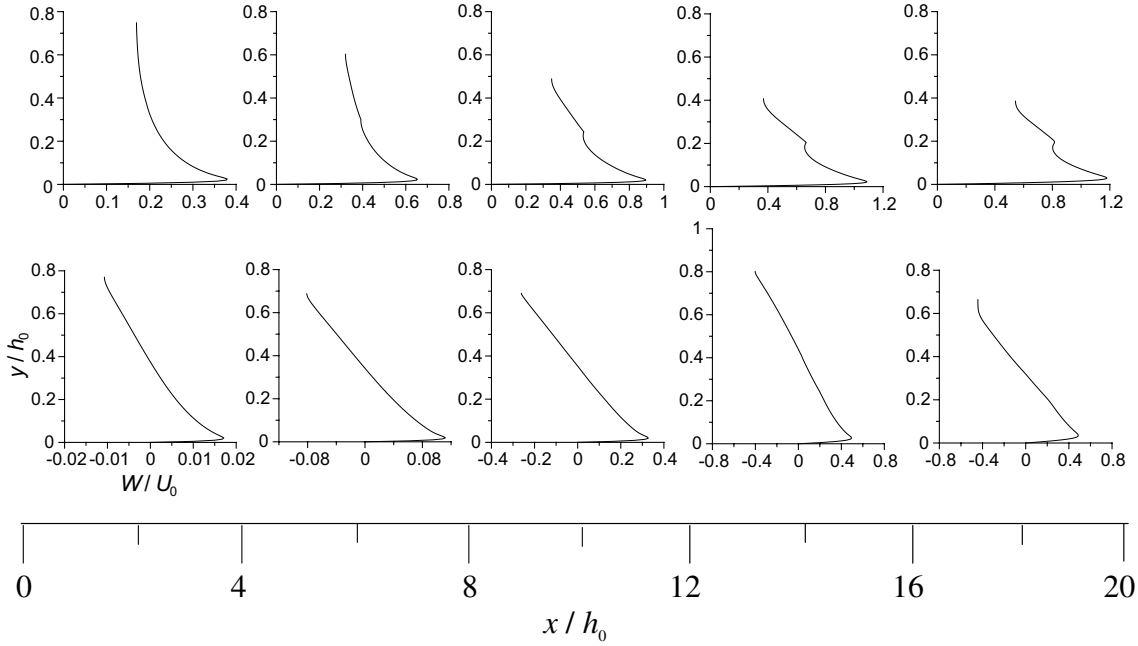

Fig. 8. Downstream variations of the azimuthal velocity component (W) in the presence of a two-component magnetic field with (upper) and without (lower) an applied electric current. See parameters in Fig. 4. $\widetilde{J} = 1.0 \times 10^{-2}$, $\widetilde{B}_y^0 = 0.002$.

induced current acts as a flow-opposing factor, while the applied one causes flow acceleration. A transition to flow regimes with acceleration by the magnetic propulsion is illustrated in Fig. 7. The propulsion force is distributed non-uniformly across the layer. It is strongest at the wall and always zero at the free surface. The intensity of the flow acceleration due to the propulsion effect

depends on the strength of the applied current. If the applied current is strong enough the flow is accelerated to the degree when it becomes even thinner than that without a magnetic field. Moreover, the calculations show that the liquid can be propelled against the gravity force. A pronounced change in the flow can be seen if the applied current has the same order of magnitude as the induced one.

Introducing a small wall-normal component of the magnetic field, B_y^0, additionally to the azimuthal field leads to a secondary flow, which is an another example of 3-D effects. A secondary flow is typically defined as the velocity component parallel to the surface of the body and perpendicular to the main flow direction. In non-MHD flows, secondary flows are associated with lateral curvature of the main flow and usually caused by the lateral pressure gradient. In flows over the body of revolution without a magnetic field, such secondary flows are afforded by the surface rotation or due to the non-zero attack angle. In the case under consideration, the secondary flow exists in the form of a swirl flow and is caused by the azimuthal Lorentz force, which arises from the interaction between the currents in the x, y plane and wall-normal magnetic field. Fig. 8 illustrates the swirl flow effect with and without an applied current. Although the wall-normal magnetic field is very small comparatively to the azimuthal field, the swirl flow is pronounced and even comparable with the main flow. Hence, the resulting flow is of a spiral type. The direction of the flow rotation depends on the current distribution. If an electric current is not applied, the azimuthal Lorentz force is fully defined by the induced currents, which are oppositely directed near the rigid boundary and free surface (see the induced current distribution in Fig. 4). Correspondingly, the liquid in the layer rotates in two opposite directions. The azimuthal velocity profile near the rigid boundary resembles that in the boundary layer. The rotation speed near the back wall is about the same as that near the free surface. The applied electric current does not suppress the swirl effect and even makes it stronger. However unlike the case with induced currents only, the applied current, if strong enough, makes the liquid to rotate in only one direction.

7. Concluding remarks

3-D thin-shear-layer equations have been derived for MHD flows. A special emphasis has been given to open-surface flows over a curved wall. The equations are formulated in terms of the 3-component velocity field and 3-component induced magnetic field. Unlike the classic boundary-layer-type equations, present ones permit information to be propagated upstream through the induced magnetic field. Another departure from the classic boundary-layer equations is that the normal momentum equation is not reduced to the simplest form, $\partial p/\partial y = 0$. Rather than that, it expresses the balance between the pressure gradient term, and those related to gravity, centrifugal forces, and the Lorentz force. Thus, the pressure variations in the normal direction are possible. Through this, the model describes a number of MHD effects related to induced axial currents, which can be caused by either spatial variations of the applied magnetic field or changes in the flow geometry. The governing equations are formulated in the orthogonal curvilinear body-oriented coordinates that allow for straightforward implementation of finite-difference techniques for calculating flows with a complex geometry. Since there are only two momentum equations in the model, which are of a marching type, the computations are much less dependent of the com-

puter power than full 3-D calculations, and as a matter of fact can be performed with a usual PC. At the same time, the model takes into account the most important 3-D effects caused by the body curvature and electromagnetic forces and gives adequate description of the flow providing the boundary-layer approximation criteria are met. The calculations were conducted for $Ha = 8500$ that has never been achieved in full 3-D computations. However at higher Ha the surface deformations are significant and the present model is inapplicable. As a next step towards higher Hartmann number flow computations one can suggest the model of ''parabolized Navier–Stokes equations'', which is still simpler than the full 3-D equations but involves much more information in comparison with the thin-shear-layer equations in the present model.

As an application of the model, flows with rotational symmetry have been considered and illustrated by numerical calculations. The applied magnetic field imitated a fusion power-reactor magnetic field varying in space as $1/r$. The calculations demonstrated MHD effects caused by a multi-component space-varying magnetic field. Two typical 3-D effects were observed, such as flow expansion (contraction) due to spatial deformations of the main flow streamlines, and a secondary flow. These effects manifest themselves in the form of a surface bump and spiral-type flow. A special consideration has been given to the magnetic propulsion effect as a tool for the active flow control by applying an external voltage. Unlike the original concept, it has been shown that the propulsion force appears not only as a result of the $1/r$-type magnetic field, but also can be caused by geometrical changes. It has been shown that the axial pressure gradient can act as an adverse pressure gradient or as a propulsion force if an external voltage is applied.

Acknowledgements

The authors would like to thank their colleagues Dr. N. Morley, Dr. B. Sreenivasan from UCLA, and Dr. L. Zakharov from PPPL for the discussions and valuable comments. This work is supported by the APEX project through DOE Grant DE-FG03-86ER52123.

References

[1] M.A. Abdou, The APEX TEAM, On the exploration of innovative concepts for fusion chamber technology, Fusion Eng. Des. 54 (2001) 181–247.
[2] T. Aitov, A. Ivanov, A. Tananaev, Flow of a liquid metal in a chute in a coplanar magnetic field, Magnetohydrodynamics 23 (1987) 91–95.
[3] F.G. Blottner, Variable grid scheme applied to turbulent boundary layers, Comput. Meth. Appl. Mech. Eng. 4 (1974) 179–194.
[4] H. Branover, Magnetohydrodynamic Flows in Ducts, Wiley, New York, 1978.
[5] T. Cebeci, Problems and opportunities with three-dimensional boundary layers, in: Three Dimensional Boundary Layers, AGARD Report No. 719, 1985, pp. 6-1–6-35.
[6] T. Cebeci, J. Cousteix, Modeling and Computation of Boundary-layer Flows, Horizons Publishing Inc., Long Beach, CA, 1999.
[7] I. Evtushenko, S. Smolentsev, A. Tananaev, Hydrodynamics and exchange of heat in thin liquid-metal layers within a magnetic field, Magnetohydrodynamics 27 (1991) 287–291.
[8] L. Howarth, The boundary layer in three-dimensional flow. Part I: derivation of the equations for flow along a general curved surface, Philos. Mag. 42 (7) (1951) 239–243.

[9] E. Kreyszig, Differential Geometry, Dover Publications, New York, 1991.
[10] V. Kudrin, S. Smolentsev, A. Tananaev, Fully developed flow of a liquid metal thin film in an inclined magnetic field, Magnetohydrodynamics 29 (1993) 66–70.
[11] L. Leboucher, Monotone scheme and boundary conditions for finite volume simulation of magnetohydrodynamic internal flows at high Hartmann number, J. Comp. Phys. 150 (1999) 181–198.
[12] A.F. Lehman, G.R. Tallbäck, H.R. Hackl, Fluid flow control in continuous casting using various configurations of static magnetic fields, in: Proceedings of International Symposium on Electromagnetic Processing of Materials, Nagoya, Japan, 25–28 October 1994, pp. 372–377.
[13] T. Levi-Civita, Allgemeine Folgerungen aus der Prandtlschen Grenzschichttheorie, in: A. Gilles, L. Hopf, Th. van Karman (Eds.), Vorträge aus dem Gebiete der Aerodynamik und verwandtewr Gebiete, Aachen, Springler, Berlin, 1929, pp. 30–50.
[14] L.G. Loitsianskii, Laminar Boundary Layer (in Russian), Nauka, Moscow, 1962.
[15] C.B. Millikan, The boundary layer and skin friction for a figure of revolution, Trans. Am. Soc. Mech. Eng. (Appl. Mech. Sect.) 54 (1932) 29–43.
[16] F.K. Moore (Ed.), Theory of Laminar Flows, Princeton University Press, Princeton, NJ, 1964.
[17] R. Moreau, Magnetohydrodynamics, Kluwer, Dordrecht, 1990.
[18] N. Morley, P. Roberts, Solutions of uniform, open-channel, liquid metal flow in a strong, oblique magnetic field, Phys. Fluids 8 (1996) 923–935.
[19] B.D. Nichols, C.W. Hirt, Calculating three-dimensional free surface flows in the vicinity of submerged and exposed structures, J. Comp. Phys. 12 (1973) 234–246.
[20] D.W. Peaceman, H.H. Rachford, The numerical solution of parabolic and elliptic differential equations, J. Soc. Ind. Appl. Math. 3 (1955) 28–41.
[21] L. Prandtl, Über Flüssigkeitsbewegung bei sehr kleiner Reibung, Verh. III, in: Intern. Mathem. Kongress, Heidelberg, 1904, pp. 484–491.
[22] L. Rosenhead (Ed.), Laminar Boundary Layers, Oxford University Press, Oxford, 1963.
[23] H. Schlichting, Boundary Layer Theory, fourth ed., McGraw-Hill Book Company Inc., New York, 1960.
[24] A.Ya. Shishko, A theoretical investigation of steady-state film flows in a coplanar magnetic field, Magnetohydrodynamics 28 (1992) 170–182.
[25] S. Smolentsev, A. Tananaev, Development of computer code for analysis of heat transfer in liquid metal MHD flows in ducts, Magnetohydrodynamics 31 (1995) 414–419.
[26] S. Smolentsev, Averaged model in MHD duct flow calculations, Magnetohydrodynamics 33 (1997) 42–47.
[27] S. Smolentsev, Mathematical models for magnetohydrodynamic flows in a fusion reactor blanket, Plasma Dev. Oper. 7 (1999) 231–241.
[28] S. Smolentsev, M. Abdou, N. Morley, A. Ying, T. Kunugi, Application of the "K–ε" model to open channel flows in a magnetic field, Int. J. Eng. Sci. 40 (2002) 693–711.
[29] A. Sterl, Numerical simulation of liquid-metal MHD flows in rectangular ducts, J. Fluid Mech. 216 (1990) 161–191.
[30] J.C. Tannehill, D.A. Anderson, R.H. Pletcher, Computational Fluid Mechanics and Heat Transfer, Taylor & Francis, London, 1997.
[31] C.E. Weatherburn, Differential Geometry of Three Dimensions, vol. I, Cambridge University Press, Cambridge, 1927.
[32] C.E. Weatherburn, Advanced Vector Analysis, Bell, London, 1944.
[33] A. Ying, M. Abdou, S. Smolentsev, H. Huang, R. Kaita, R. Maingi, N. Morley, B. Nelson, T. Sketchley, M. Ulrickson, R. Woolley, MHD and heat transfer issues and characteristics for Li free surface flows under NSTX conditions, Fusion Technol. 39 (2001) 739–745.
[34] L. Zakharov et al., Magnetic propulsion of conducting fluid and the theory of controlled tokomak fusion reactor, Meeting on Liquid Lithium, Controlled Tokamak Fusion Reactors and MHD, Int. Sherwood Fusion/Plasma Conf., Atlanta, GA, March 21, 1999.